Thermochemistry of glasses along the $2NdAlO_3$–$3SiO_2$ join

2003 J. Phys.: Condens. Matter 15 S2343

(http://iopscience.iop.org/0953-8984/15/31/310)

INSTITUTE OF PHYSICS PUBLISHING JOURNAL OF PHYSICS: CONDENSED MATTER

J. Phys.: Condens. Matter **15** (2003) S2343–S2355 PII: S0953-8984(03)60999-9

Thermochemistry of glasses along the $2NdAlO_3$–$3SiO_2$ join

Yahong Zhang[1], **Alexandra Navrotsky**[1], **Jean A Tangeman**[2] **and J K Richard Weber**[2]

[1] Thermochemistry Facility and NEAT ORU University of California at Davis, Davis, CA 95616, USA
[2] Containerless Research, Inc., 906 University Place, Evanston, IL 60201, USA

Received 18 March 2003
Published 23 July 2003
Online at stacks.iop.org/JPhysCM/15/S2343

Abstract

Five Nd–aluminosilicate glasses along the $2NdAlO_3$–$3SiO_2$ join were synthesized using conventional drop-quench techniques. A sixth glass, with the end-member $NdAlO_3$ composition, required synthesis by containerless liquid-phase processing methods to avoid crystallization. Enthalpies of drop solution (ΔH_{ds}) and formation (ΔH_f) for the Nd–aluminosilicate glasses and the $NdAlO_3$-composition end-member glass were measured in molten $2PbO$–B_2O_3 at 1078 K in a twin Calvet type calorimeter. Values for ΔH_{ds} for the Nd–aluminosilicate glasses increase with decreasing silica content from 130.7 ± 1.5 to 149.6 ± 0.6 kJ mol^{-1}. Similarly, values of ΔH_f increase with decreasing silica content from 41.0 ± 2.0 to 59.0 ± 1.6 kJ mol^{-1}. Values of ΔH_{ds} and ΔH_f for $NdAlO_3$-composition glass were measured as 99.3 ± 0.9 and 139.2 ± 2.1 kJ mol^{-1}, respectively. Using transposed temperature drop calorimetry, the enthalpy of vitrification for $NdAlO_3$-composition glass was measured as 69.5 ± 0.9 kJ mol^{-1} relative to the stable crystalline neodymium aluminium perovskite ($NdAlO_3$) phase. Enthalpies of mixing were calculated based on amorphous end members; the strongly negative values support the absence of immiscibility in this system. Differential scanning calorimetry was used to determine glass transition (T_g) and crystallization (T_x) temperatures, as well as values for the configurational heat capacity ($\Delta C_P(T_g)$) and the temperature range of the supercooled liquid interval ($\Delta T(SCL)$). The $NdAlO_3$-composition glass showed no evidence of a glass transition prior to crystallization; only a single exotherm was observed, the onset of which occurred at 1045 K. For the Nd–aluminosilicates, values of T_g and $\Delta T(SCL)$ increase with increasing silica content, from 1128 to 1139 K and from ∼95 to ∼175 K, respectively. Values of ($\Delta C_P(T_g)$) increase with decreasing silica content, from ∼27 to ∼75 J/g fw *K, reflecting the increasing fragility and decreasing stability of the liquids as the end member composition, $NdAlO_3$, is approached.

1. Introduction

Rare earth aluminosilicate glasses exhibit somewhat anomalous, yet often desirable, physical properties such as high glass transition temperatures, high values of hardness and elastic modulus and excellent chemical durability [1, 2]. In recent years, Nd- and Er-doped glasses and glass fibres have received considerable attention as laser hosts and as optical amplifiers in all-optical long-distance telecommunication fibre networks [3, 4]. However, high field strength cations, such as the rare earths, exert a control on the bulk structure of high silica glasses and liquids [5] by defining their own coordination environments [6, 7]. Clustering and nanometre-scale phase separation appear to occur in silica-rich host glasses doped with ppm levels of rare earth oxides [8]. This heterogeneity dramatically lowers the optical amplification efficiency of glass fibres. Understanding the inhomogeneous distribution of cations is also important for optimizing nuclear waste from processing where rare earth elements are added as surrogates for actinides, as fission products and as neutron absorbers [9, 10].

Miscibility gaps in silicate melts and glasses occur as both stable and metastable features [11]. The bulk thermodynamics may thus reflect whether a heterogeneous distribution of rare earth ions exists on a molecular scale. Evidence has been presented for incipient phase separation in lanthanum-containing silicate liquids [12] and gadolinium- or hafnium-doped sodium alumino-borosilicate glasses [13] by using the techniques of high temperature oxide melt solution calorimetry. Spectroscopic studies show that co-doping rare earth silicate glasses with similar concentrations of Al_2O_3 or P_2O_5 appears to produce a homogeneous distribution of rare earth cations, even at high concentration levels [14]. To obtain thermochemical evidence for this apparent stabilization of glasses containing both rare earth and aluminium ions, we measured the enthalpies of formation and of mixing of glasses along the neodymium aluminate–silica join. Differential scanning calorimetry was performed to determine transition temperatures (i.e. glass transition and crystallization) and values for the configurational heat capacities and supercooled liquid (SCL) temperature intervals. The compositions are expressed throughout this paper as $2NdAlO_3$–$3SiO_2$ (rather than $NdAlO_3$–SiO_2) to refer to a constant number of oxygen atoms in the system. This particular series was chosen as it lies in the middle of the single-phase glass forming region [15]. These compositions are also of interest for alumina–rare earth aluminate eutectic materials applied to ceramic microwave devices [16, 17] and for multi-component engineering ceramics based on Si_3N_4 and SiAlON [18–20].

2. Experimental details

2.1. Sample synthesis and characterization

Glasses along the $2NdAlO_3$–$3SiO_2$ join were prepared by mixing appropriate amounts of reagent grade Al_2O_3 (Alfa, 99.99%), silicic acid (Aldrich, 99.9%) and Nd_2O_3 (Alfa, 99.99%) powders. As silicic acid and Nd_2O_3 are hygroscopic, their water contents were determined through thermogravimetric experiments and weight corrections were applied.

Synthesis of the end-member $NdAlO_3$-composition glass was accomplished using containerless, liquid-phase processing techniques. Two grams of the mixed oxide powder was fused in a laser hearth [21], crushed to a powder, re-fused, and then crushed into pieces $\sim$1.5 mm in diameter. The crystalline pieces were levitated in a stream of pure oxygen, and melted using a continuous-wave CO_2 laser. The molten, levitating droplets were cooled by blocking the laser beam. Cooling rates sufficient to result in vitrification of the molten levitating droplet were achieved by processing pieces of the precursor material which were 1.5 mm or less in diameter (the smaller the spheroid, the faster the cooling rate). Both the relatively rapid cooling rate and the absence of container surfaces on which crystals could nucleate contributed

to successful glass formation. A portion of the $NdAlO_3$-composition glass was crystallized by heat treatment above its crystallization temperature, which was determined through scanning calorimetric experiments.

Silica-containing compositions were melted in air in an uncovered Pt crucible with a thick Pt wire handle, which was suspended by a thin Pt wire in a vertical tube furnace (Deltech). After 30 min in the furnace at 1923 K, the liquid was quenched by dropping the Pt crucible into deionized water below the furnace. The crucible dropped after passing current through the Pt wire, causing it to melt at the thinnest point, i.e. the thin suspension wire.

All glasses and crystalline $NdAlO_3$ were first examined with a Scintag PAD-V diffractometer operated at 45 kV and 40 mA using Cu Kα radiation and calibrated using quartz as a standard. Chemical compositions were analysed using a Cameca SX-50 electron microprobe. Quantitative, wavelength-dispersive analyses of all glasses in the suite and crystalline $NdAlO_3$ were performed at 20 keV with a beam current of 10 nA using an approximately 1 μm diameter electron beam and $NdPO_4$, SiO_2 and Al_2O_3 standards for Nd, Si and Al.

2.2. Calorimetry

To determine enthalpies of formation, high temperature drop solution calorimetry was performed in a Calvet-type twin calorimeter described by Navrotsky [22, 23]. Powdered glass samples weighing 15 mg were pressed into pellets and dropped from room temperature into a molten $2PbO$–B_2O_3 solvent at 1078 K. Heat flow was measured as a voltage change in the thermopile. The integrated voltage versus time curve was converted to enthalpy by application of a calibration factor based on the heat content of α-Al_2O_3 of similar mass.

The enthalpy of vitrification for $NdAlO_3$-composition glass at 298 K was measured by a two-step transposed temperature drop calorimetric experiment. Pellets of powdered glass ($\sim$15 mg) were dropped from room temperature (298 K) into an empty Pt crucible in the calorimeter at 1078 K, and the heat effect was measured. The devitrified sample was then removed from the Pt crucible and its heat content was measured by a second set of transposed temperature drop experiments, performed in a similar manner. The difference between the two sets of experiments gives the enthalpy of vitrification.

To determine heat capacities, glass transition temperatures, SCL ranges and crystallization temperatures, differential scanning calorimetry (DSC) experiments were conducted using a Netzsch DSC-404 calorimeter. About 40 mg of powdered glass was placed in a platinum pan before loading into the calorimeter. Continuous scans of the baseline (empty Pt crucible), standard (α-Al_2O_3) and sample were performed at a scan rate of 20 K min^{-1} in flowing argon up to 1673 K. Baseline corrections were applied to both the standard and sample runs. The calibration curves were obtained by using measured values of the baseline-corrected alumina standard in conjunction with accepted values for the heat capacity of α-Al_2O_3 [24]. Heat capacities of the glasses from 298–1673 K were then calculated (using the Netzsch software package) by applying the calibration curve to the baseline-corrected sample measurement. This methodology for CP determination is similar to that described by Mraw [25].

3. Results

3.1. Glass formation, enthalpy of vitrification and formation from oxides for the $NdAlO_3$ end member

Pieces, approximately 1–1.5 mm diameter, of the hearth-melted crystalline $NdAlO_3$ formed glass relatively easily under containerless conditions. The glass was purple in colour, and the

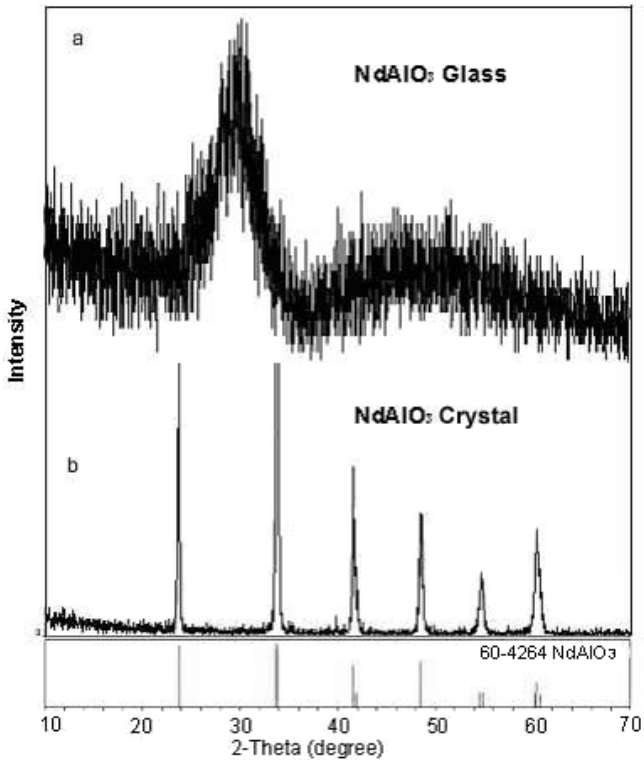

Figure 1. XRD pattern for amorphous and crystalline $NdAlO_3$.

Table 1. Nominal and analysed compositions of glasses along the $2NdAlO_3$–$3SiO_2$ join, based on a six-oxygen formula unit.

	Nominal			Analysed		
Sample	Nd	Si	Al	Nd	Si	Al
Glasses						
Nd1010	0.60	2.10	0.60	0.61	2.12	0.57
Nd1515	0.80	1.80	0.80	0.85	1.77	0.78
Nd2020	1.00	1.50	1.00	0.96	1.52	1.01
Nd2525	1.20	1.20	1.20	1.13	1.26	1.19
Nd3030	1.40	0.90	1.40	1.32	0.95	1.42
Nd5050	2.00	—	2.00	2.02	—	1.98
Crystal						
Nd5050	2.00	—	2.00	1.99	—	2.01

majority of the glass spheroids contained a single internal fully enclosed bubble that formed upon cooling in the levitator. As illustrated by the absence of Bragg peaks in the XRD pattern (figure 1(a)), the resulting sample is fully amorphous and the nominal and measured compositions of the glass are in excellent agreement (Nd5050 in table 1).

DSC performed on the glass revealed only one exothermic phase transition. X-ray diffraction on the material resulting from this exothermic event showed that it was phase-pure $NdAlO_3$ perovskite (figure 1(b)), demonstrating that the heat release was due to crystallization. No transition endotherms, most notably no glass transition, were observed in the calorimetric

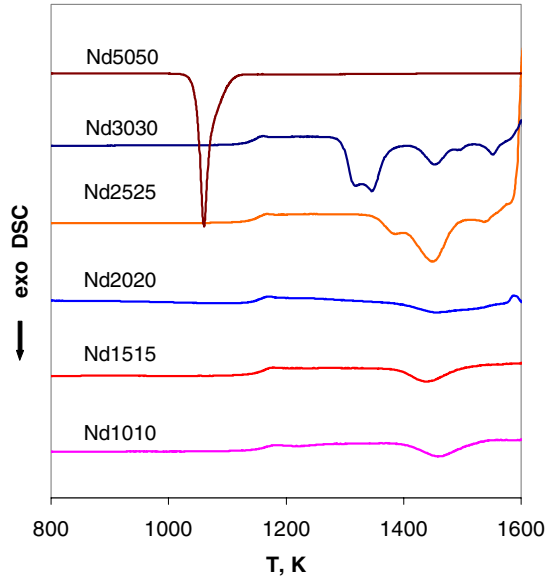

Figure 2. DSC traces for glasses along the $2NdAlO_3$–SiO_2 join measured at 20 K min^{-1}. (This figure is in colour only in the electronic version)

trace over the entire temperature range of measurement. It is noted that an attempt was made to 'unmask' at least some evidence of the glass transition by performing a scan on the intact glass spheroids, in addition to the powdered glass. Still, no T_g endotherm was observed, but crystallization of the glass spheroids occurred at a temperature ∼100 K higher than that for the glass in powder form. The onset of crystallization for $NdAlO_3$-composition glass (powdered) occurred at 1045 K (Nd5050 in figure 2). Because 1045 K is lower than the temperature of 1078 K of the Calvet-type twin calorimeter used for enthalpy determinations, and because $NdAlO_3$-composition glass crystallizes to phase-pure $NdAlO_3$ perovskite, transposed temperature drop experiments could be performed, as described below, to determine the enthalpy of vitrification of this material.

The enthalpy of vitrification at 298 K for $NdAlO_3$ was measured by a two-step transposed temperature drop calorimetric technique (table 2). In the first step, $NdAlO_3$ glass readily devitrified in the calorimeter at 1078 K into single-phase perovskite on the timescale of experiments (∼1 h), as verified by electron microprobe analysis and XRD experiments (figure 1(b)), which show a good fit of the measured spectrum to the reference pattern [26] for $NdAlO_3$. The heat effect measured in the first step, or first set of drops, is 31.0 ± 0.4 kJ mol^{-1}, which is equal to the heat content of the glass ($H_{1078} - H_{298}$) plus the heat of devitrification. In the second part of the transposed temperature drop experiment, the devitrified sample (phase-pure $NdAlO_3$ perovskite) was removed from the Pt crucible and then its heat content was measured by dropping 15 mg pellets of the recovered material into the calorimeter at 1078 K, resulting in a value of 100.5 ± 0.8 kJ mol^{-1}. The difference between the values obtained in the two parts of the transposed temperature drop experiment gives the enthalpy of vitrification of $NdAlO_3$ as 69.5 ± 0.9 kJ mol^{-1} at 298 K.

By measuring the enthalpy of the drop solution of $NdAlO_3$ glass in molten lead borate and using appropriate thermochemical cycles (table 2), we calculated the enthalpy of formation for amorphous $NdAlO_3$ from crystalline oxides at 298 K to be 17.7 ± 1.2 kJ mol^{-1}. Using the

Table 2. Thermochemical cycles.

Reaction	ΔH^{a} (kJ mol^{-1})
(1) $NdAlO_3$ (glass, 298 K) → $NdAlO_3$ (xtal, 1078 K)	31.0 ± 0.4 (8)
(2) $NdAlO_3$ (xtal, 298 K) → $NdAlO_3$ (xtal, 1078 K)	100.5 ± 0.8 (6)
(3) $NdAlO_3$ (glass, 298 K) → $1/2Nd_2O_3$ (dissolved, 1078 K) + $1/2Al_2O_3$ (dissolved, 1078 K)	49.6 ± 0.4 (8)
(4) Nd_2O_3 (xtal, 298 K) → Nd_2O_3 (dissolved, 1078 K)	14.3 ± 0.9 (6)
(5) Nd_2O_3 (xtal, 1078 K) → Nd_2O_3 (dissolved, 1078 K)	-89.1 ± 0.7 (7)
(6) Al_2O_3 (xtal, 298 K) → Al_2O_3 (dissolved, 1078 K)	120.4 ± 0.5 (8)
(7) Al_2O_3 (xtal, 298 K) → Al_2O_3 (xtal, 1078 K)	87.6[b]
(8) $(1-x)2NdAlO_{3-x}(3SiO_2)$ (glass, 298 K) → $(1-x)/2Nd_2O_3$ (dissolved, 1078 K) $+3xSiO_2$ (dissolved, 1078 K) $+(1-x)/2Al_2O_3$ (dissolved, 1078 K)	ΔH_8
(9) SiO_2 (α-quartz, 298 K) → SiO_2 (dissolved, 1078 K)	47.9 ± 0.6
(10) $NdAlO_3$ (xtal, 298 K) → $NdAlO_3$ (glass, 298 K) $\Delta H_{10} = -\Delta H_1 + \Delta H_2$	69.5 ± 0.9
(11) $1/2Nd_2O_3$ (xtal, 298 K) $+1/2Al_2O_3$ (xtal, 298 K) → $NdAlO_3$ (glass, 298 K) $\Delta H_{11} = -\Delta H_3 + \Delta H_4/2 + \Delta H_6/2$	17.7 ± 1.2
(12) $1/2Nd_2O_3$ (xtal, 298 K) $+1/2Al_2O_3$ (xtal, 298 K) → $NdAlO_3$ (xtal, 298 K) $\Delta H_{12} = -\Delta H_3 + \Delta H_4/2 + \Delta H_6/2 + \Delta H_{10}$	-52.2 ± 1.4
(13) $1/2Nd_2O_3$ (xtal, 1078 K) $+1/2Al_2O_3$ (xtal, 1078 K) → $NdAlO_3$ (xtal, 1078 K) $\Delta H_{13} = \Delta H_1 - \Delta H_3 + \Delta H_5/2 + (\Delta H_6 - \Delta H_7)/2$	-46.5 ± 0.8 -43.4 ± 2.9[c]
(14) $(1-x)(2NdAlO_3)$ (xtal, 298 K) $+ x(3SiO_2)$ (α-quartz, 298 K) → $(1-x)(2NdAlO_3) - x(3SiO_2)$ (glass, 298 K) $\Delta H_{14} = -\Delta H_8 + 2(1-x)\Delta H_{12} + 3x\Delta H_9$	ΔH

[a] Uncertainty is two standard deviations of the mean; the number in parentheses is the number of experiments.
[b] Calculated from [32].
[c] Enthalpy of formation from oxides at 977 K [34] recalculated using Nd_2O_3 data from current study.

enthalpy of vitrification for $NdAlO_3$, the enthalpy of formation of crystalline $NdAlO_3$ from binary oxides was determined as -52.2 ± 1.4 kJ mol^{-1}.

3.2. Glass formation and characterization of the Nd–aluminosilicates

All five compositions in the Nd–Al–Si–O system formed transparent single-phase bulk glasses using the drop-quench technique. The glasses were purple in colour, like the $NdAlO_3$-composition glass, and no Bragg peaks were observed in the XRD patterns, indicating that the resulting samples were fully amorphous. As shown in table 1, the nominal and measured compositions of the glasses are in excellent agreement.

3.3. Differential scanning calorimetric results for the Nd–aluminosilicate glasses

The differential scanning calorimetric traces for the silica-bearing glasses in the Nd–Al–Si–O suite are shown in figure 2, along with the scan for $NdAlO_3$ composition glass (figure 2). Except for the $NdAlO_3$ composition, all of the glasses in this study exhibit an endothermic slope change that corresponds to the glass transition. Along the $2NdAlO_3$–$3SiO_2$ join, the glass transition temperatures (determined as the onset of the slope change) increase only slightly, but linearly with increasing SiO_2 content (figure 3) from 1128 K for Nd3030 to 1139 K for Nd1010. At temperatures above the glass transition, the SCL regime is accessed. When this liquid crystallizes, one or more exothermic events are observed, depending on the

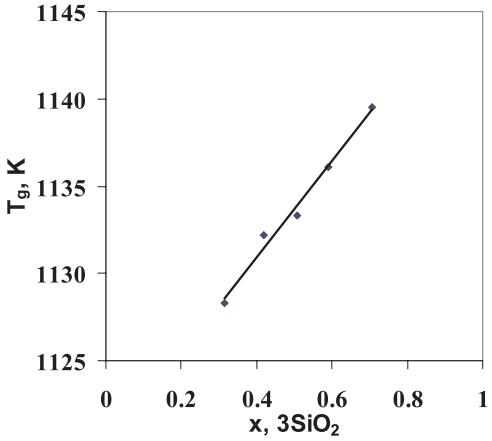

Figure 3. Onset glass transition temperatures for glasses along the $2NdAlO_3$–$3SiO_2$ join. The full line is a linear fit: $T_g = 27.79x + 846.76$, $R^2 = 0.9862$.

composition. The Nd–aluminosilicates containing the smallest amount of silica, Nd3030 and Nd2525, show the briefest SCL interval, ∼95 and 150 K, respectively and the most complex crystallization path, with multiple exotherms. The SCL regime for compositions Nd2020, Nd1515 and Nd1010 persists for approximately 175 K, a significantly greater temperature interval than for the other two. When liquids of these latter compositions crystallize, only one exotherm is clearly discerned. The increase in heat capacity at the glass transition, also known as the configurational heat capacity $\Delta C_P(T_g)$, increases markedly with decreasing silica content for the Nd–aluminosilicates. Values of $\Delta C_P(T_g)$ range from 27 J/g fw *K for Nd1010 (80 mol% SiO_2) to the rather high value of 75 J/g fw *K for Nd3030 (40 mol% SiO_2), where g fw = ΣXiMWi.

3.4. Enthalpies of drop solution and enthalpies of formation from crystalline end members, $NdAlO_3$ (perovskite) and SiO_2 (quartz)

All samples dissolved in molten lead borate in a reasonable time (∼50 min). Enthalpies of drop solution (table 3) become strongly endothermic as silica content increases, reaching a maximum near $x = 0.35$ (mole fraction of $3SiO_2$), and then curve back to more exothermic values as shown in figure 4. A third-order polynomial was fitted to the data, and this curve and the fitted equation are shown in figure 4.

The enthalpies of formation (ΔH_f) were calculated with respect to their crystalline end member oxides at 298 K based on their drop solution enthalpies in lead borate solvent (see cycles in table 2). Values of ΔH_f for the five Nd–aluminosilicate glasses, $NdAlO_3$-composition glass and α-quartz are plotted against the mole fraction of $3SiO_2$ in figure 5. The best-fit curve through the data is a third-order polynomial and is shown in figure 5.

There is a dramatic change in the slope in the enthalpies of formation from crystalline end members versus silica content between low-silica glasses and glasses with silica contents greater than approximately 45 mol%. The glasses are stabilized with the addition of silica as shown by the sharp decrease in the values of ΔH_f by ∼100 kJ mol^{-1} from the end-member $NdAlO_3$-composition glass to the silica-containing glasses. The enthalpies of formation are nearly composition independent for glasses with silica contents between ∼45 and 80 mol%. As the silica content approaches 100%, the enthalpies of formation become slightly more exothermic.

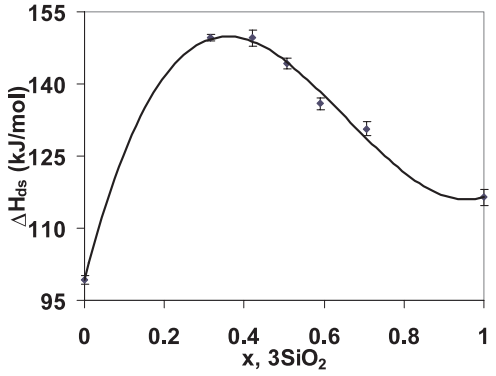

Figure 4. Enthalpies of drop solution in molten lead borate for glasses along the $2NdAlO_3$–$3SiO_2$ join. The full curve is a third-order polynomial fit: $\Delta H_{ds} = (324.1 \pm 23.6)x^3 - (633.4 \pm 33.4)x^2 + (326.7 \pm 11.8)x + (99.3 \pm 1.2)$, $R^2 = 0.998$.

Table 3. Enthalpies of drop solution in molten lead borate for oxides, enthalpies of formation from crystalline end members and enthalpies of mixing at 298 K from glass end members.

Glass	Mole fraction $3SiO_2$	ΔH_{ds}[a] (kJ mol^{-1})	ΔH_f (kJ mol^{-1})	ΔH_{mix} (kJ mol^{-1})
$3SiO_2$	1	116.4 ± 1.7	27.4 ± 2.4	0.0 ± 2.4
Nd1010	0.7	$130.7 \pm 1.5(8)$	41.0 ± 2.0	-19.3 ± 1.9
Nd1515	0.6	$136.0 \pm 1.2(6)$	46.5 ± 1.8	-26.6 ± 1.6
Nd2020	0.5	$144.3 \pm 1.2(6)$	46.1 ± 1.7	-36.4 ± 1.5
Nd2525	0.4	$149.6 \pm 1.6(6)$	49.1 ± 2.1	-43.1 ± 1.9
Nd3030	0.3	$149.6 \pm 0.6(6)$	59.0 ± 1.6	-44.9 ± 1.0
Nd5050	0	$99.3 \pm 0.9(8)$	139.2 ± 2.1	0.0 ± 1.2
Crystal:	ΔH_{ds}[a] (kJ mol^{-1})	Crystal:	ΔH_{ds}[a] (kJ mol^{-1})	
SiO_2	47.9 ± 0.6 (8)	Al_2O_3	120.4 ± 0.6 (8)	
Nd_2O_3	14.3 ± 0.9 (7)	$NdAlO_3$	119.2 ± 1.0 (6)	

[a] Uncertainty is two standard deviations of the mean; the number in parentheses is the number of experiments.

3.5. Enthalpies of mixing from glassy end members, $NdAlO_3$ and SiO_2, at 298 K

The enthalpies of mixing were determined from the difference between the ideal enthalpy of drop solution (a linear combination of the end-member enthalpies) and the measured enthalpy of drop solution. In figure 6, the broken line indicates zero heat of mixing while the full curve represents a third-order polynomial fit, the equation for which is shown in figure 6. The fitted curve is asymmetric, reaching a minimum at $x = 0.35$. Enthalpies of mixing from glassy end members are negative throughout the composition range studied.

4. Discussion

4.1. Vitrification and enthalpy of formation for $NdAlO_3$

The only stable crystalline phase that forms from Nd_2O_3 and Al_2O_3 is neodymium aluminium perovskite ($NdAlO_3$) [27]. By comparison, the more widely studied yttrium and erbium aluminates form stable garnet $M_3Al_5O_{12}$ and monoclinic $M_4Al_2O_9$ phases in addition to

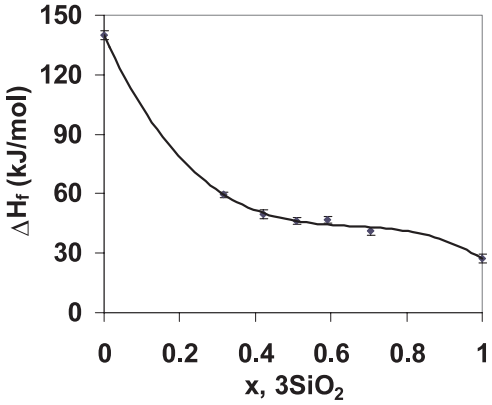

Figure 5. Enthalpies of formation from crystalline end members at 298 K for glasses along the $2NdAlO_3$–$3SiO_2$ join. The full curve is a third-order polynomial fit: $\Delta H_f = (-319.6 \pm 30.1)x^3 + (626.7 \pm 45.3)x^2 - (419.7 \pm 17.8)x + (139.7 \pm 2.1)$, $R^2 = 0.998$.

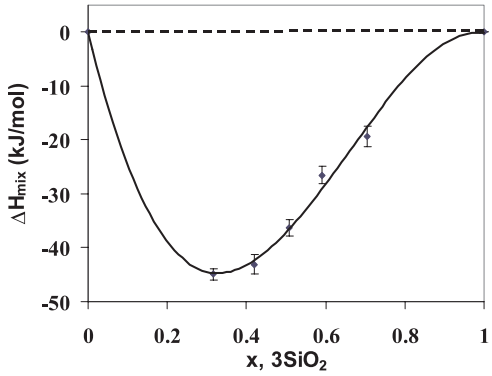

Figure 6. Enthalpies of mixing at 298 K for glasses along the $2NdAlO_3$–$3SiO_2$ join. The broken line represents the ideal ΔH_{mix} while the full curve represents a third-order polynomial fit: $\Delta H_{mix} = (-323.3 \pm 25.8)x^3 + (632.2 \pm 36.9)x^2 - (309.2 \pm 13.2)x$, $R^2 = 0.997$.

perovskite [28]. Crystallization and non-equilibrium phase formation in the yttrium oxide–aluminium oxide pseudobinary materials has been investigated by several authors [29–31]. Glass formed from the $Y_3Al_5O_{12}$ composition has an enthalpy of vitrification of 276.5 ± 5.4 kJ mol^{-1} [33], which is strikingly similar to that of $NdAlO_3$ measured in this study (277.9 ± 3.4 kJ mol^{-1} for 12 oxygen basis). The integration of the crystallization exotherm observed in the heat capacity curve resulted in a value of enthalpy of vitrification of 63.3 ± 2.0 kJ mol^{-1}, in reasonable agreement with the more accurate transposed temperature drop calorimetry experiments (69.5 ± 0.9 kJ mol^{-1}). This high value of the enthalpy of vitrification is reflected in the strong tendency toward crystallization during glass synthesis for the $NdAlO_3$ composition.

Kanke and Navrotsky [34] investigated the thermochemistry of binary rare earth oxide aluminates, including the crystalline perovskite phases. Their value for the enthalpy of formation for crystalline $NdAlO_3$ at 977 K is -41.4 ± 3.4 kJ mol^{-1}. This difference from our value of -46.5 ± 0.8 kJ mol^{-1} might arise from errors in their value for the enthalpy of solution for Nd_2O_3. Because their experiments were performed at a calorimeter temperature of 977 K, their sample was mixed with CuO to enhance the dissolution rate at this lower temperature.

In addition, the hygroscopic nature of Nd_2O_3 was not considered. The Nd oxide used in the current experiments had a weight loss of nearly 15% after firing. The present drop solution data for Nd_2O_3 at 1078 K was cross-checked with a combination of transposed temperature drop and solution experiments ($\Delta H_{ds} = H_{TTD} + \Delta H_s$) with the new 'air gun' technique [35]. Using the enthalpy of solution from the current study, Kanke *et al*'s enthalpy of formation from the oxides at 977 K was recalculated to be -43.4 ± 2.9 kJ mol^{-1}, which is in good agreement with our value at 1078 K: -46.5 ± 0.8 kJ mol^{-1} (table 2).

4.2. Features of the glass transition region and the supercooled liquid regime

Rare earth aluminosilicate glasses have relatively high glass transition temperatures compared to conventional mono- or divalent oxide-doped aluminosilicate glasses. This may be a result of the stronger bonding of the trivalent cations and the lower contrast in bond strengths between bridging and non-bridging oxygen (NBO) bonds involving rare earth ions. According to Ray [36], the glass transition temperature in an oxide glass is related to the density of covalent crosslinking, the number and strength of the coordinate links formed between oxygen and the cation and the oxygen density of the network. Higher values of these factors correspond to higher glass transition temperatures. For glasses along the $2NdAlO_3$–$3SiO_2$ join, with increasing $NdAlO_3$ content, more coordinate links are formed between oxygen and Nd. This effect is opposed by

(1) the lower oxygen density of the network resulting from the more open structure needed to accommodate larger neodymium ions, and
(2) depolymerization in the network with decreasing silica content.

Reflecting this competition of factors, the glass transition temperature displays a slight increase with increasing silica content along the $2NdAlO_3$–$3SiO_2$ join from 1128 to 1139 K (figure 3). If this trend of T_g versus silica content for the Nd–aluminosilicate glasses were extrapolated, the T_g value for the $NdAlO_3$-composition glass would be 1120 K J/g fw *K. The DSC traces in figure 2 suggest that increasing $NdAlO_3$ content greatly destabilizes the liquids with regard to devitrification, while the glass transition temperature changes by only a few degrees. This effect is particularly obvious in the silica-poor region, which corresponds to the sharp energetic destabilization with decreasing silica content in enthalpies of formation from crystalline end member oxides (figure 4).

The configurational heat capacities for the Nd–aluminosilicate glasses increase markedly with decreasing silica content. The $\Delta C_P(T_g)$ for the Nd3030 composition glass, with 40 mol% SiO_2 reaches a value of $\sim$75 J/g fw *K. This value is comparable to that of silica-free, single-phase Y-aluminate glasses, which have values of $\Delta C_P(T_g)$ as high as 81 J/g fw *K [31]. These high values are a reflection of the extreme fragility of the liquids and the increasing difficulty of glass formation with decreasing silica content. No T_g endotherm is observed for the $NdAlO_3$-composition glass in the DSC trace in figure 2. However, if the trend of $\Delta C_P(T_g)$ versus silica content, which is determined from the other five glasses in this study, were extrapolated, the $\Delta C_P(T_g)$ value for the $NdAlO_3$-composition glass would be $\sim$120 J/g fw *K. This high, albeit extrapolated, value may be an indication that the liquid is so fragile, and so unstable with increasing temperature, that the tendency toward crystallization is irrepressible, effectively preventing expression of the glass transition. Paralleling this result is the observation that the SCL range decreases substantially with decreasing silica content. If the observed trend of the temperature interval of the SCL regime versus silica for the Nd–aluminosilicate glasses is extrapolated to the $NdAlO_3$ composition, the SCL temperature range for this end-member is a

large negative value, further support for the interpretation that the $NdAlO_3$-composition liquid is extremely unstable toward crystallization and highly fragile.

4.3. Enthalpies of mixing

In binary liquid solutions, a zero heat of mixing is often taken to indicate Raoultian (ideal) behaviour. Deviations from such behaviour are seen as positive heats of mixing, which drive the solution towards immiscibility (e.g. in the silica-rich regions of binary alkali silicate liquids [37]) or negative heats of mixing (complex formation in a homogeneous single liquid). The enthalpies of mixing for glasses along the $2NdAlO_3$–$3SiO_2$ join are asymmetric and significantly negative (figure 6), indicating sub-regular solution behaviour and an absence of immiscibility. While the maximum stabilization occurs at or near $Al/Si = 1$ for fully polymerized glasses [38], this trend also appears to apply to less polymerized glasses like these along the $2NdAlO_3$–$3SiO_2$ join, where maximum stabilization occurs at about $x = 0.35$ (near $Al/Si = 1$) (figure 6). This may be related to the energetics of the reaction Al–O–Al + Si–O–Si = 2Al–O–Si [39], which suggests the Al–O–Si linkage is stable relative to a mixture of Si–O–Si and Al–O–Al linkages for the system studied.

A high temperature solution calorimetry study by Wilding *et al* [13] of La_2O_3 in a series of rare earth–alkali–alkaline earth silicate liquids suggests that La(III) ions form incipient phase-ordered regions. The enthalpies of drop solution vary linearly with composition in the glass formation region. A Raman spectroscopic study by Ellison and Hess [40] implies disruption of the transient silicate network and coordination of La(III) to free oxygen in K_2O–La_2O_3–SiO_2 glasses. This is also supported by an NMR study by Schaller *et al* [41]. The strong interaction between the rare earth ions, R, and oxygen in such a network structure may cause formation of R–O–R clusters coexisting with Si–O–Si structures, eventually leading to phase separation [42, 43]. Such bonding environments may become energetically unstable on introduction of Al or P in the glass structure, resulting in a homogeneous dispersion of the rare earth ions with the formation of R–O–Al or R–O–P types of links [44]. Sen [45] carried out Nd and Al EXAFS studies and found that the homogenization is manifested by a marked increase in Nd–O distance, giving rise to volume relaxation of the Nd–O coordination polyhedra. The formation of Nd–O–Si and Nd–O–Al bonds at the expense of Nd–O–Nd bonds indicates incorporation of Nd–O coordination polyhedra into the aluminosilicate network. Structural studies with FTIR, neutron scattering and small-angle x-ray scattering on glasses along the $2NdAlO_3$–$3SiO_2$ join are in progress and will be discussed elsewhere. In contrast to the alumina-free glasses and melts studies by Wilding *et al* [13], the $2NdAlO_3$–$3SiO_2$ glasses show strongly negative heats of mixing, indicating, as pointed out above, a significant stabilization near $Al/Si = 1$. Though the details of Al coordination (AlO_5, AlO_5, AlO_6) and of Nd–O bonding or possible clustering are not yet known for this system, the strongly negative heats of mixing suggest a large thermodynamically favoured glass forming region in which all ions are in relatively low energy coordination environments. There is no thermodynamic evidence for phase separation except possibly at very high silica content.

The actual distribution of rare earth ions and NBOs between the tetrahedral and non-tetrahedral volumes of these aluminosilicate glasses is not yet known and there may be a change of such volumes across the system. Interpretation of enthalpies of mixing to develop structural models is very difficult, considering the relative scarcity of data and the fact that thermodynamic data are sensitive only to significant changes in average structural properties. The third-order polynomials used for fitting purposes in this work do not have a physical significance in terms of glass structure. Corrales [46] used molecular dynamics simulations to examine the driving force for immiscibility in binary silicates [47]. A set of systematic

thermochemical data, combined with structural data, would provide experimental validation for such molecular dynamics computer simulations of rare earth aluminosilicate glasses. These calorimetric data can also be fed into CALPHAD (calculation of phase diagrams) type software packages to optimize the phase diagram [48, 49]. The thermodynamic properties of subsystems of the whole ternary system can then be calculated and extrapolated into more complex higher-component systems.

5. Conclusions

Five silica-containing glasses along the $2NdAlO_3$–$3SiO_2$ join were synthesized using conventional drop-quench techniques, while the end-member $NdAlO_3$-composition glass required synthesis with containerless methods due to its tendency to crystallize during liquid phase processing. The high value for the enthalpy of vitrification of $NdAlO_3$-composition glass at 298 K, 69.5 ± 0.9 kJ mol^{-1}, which is based on transposed temperature drop calorimetric experiments, reflects the reluctant glass-forming tendency of this material. High temperature oxide melt calorimetry was performed on all six glasses along the $2NdAlO_3$–$3SiO_2$ join to determine the energetic stabilization of the glasses. Asymmetric negative enthalpies of mixing substantiated stabilization with sub-regular solution behaviour and the absence of immiscibility in the composition range studied. DSC revealed only a slight decrease in T_g with decreasing silica content, but a marked increase in the configurational heat capacities with decreasing silica and a corresponding substantial decrease in the temperature range of the SCL region. These characteristics lend support to the interpretation that, with increasing $NdAlO_3$ content, the liquids become increasingly destabilized until, at the $NdAlO_3$ end-member composition, no T_g endotherm is observed, because the liquid has become unstable enough to render the glass transition kinetically unfavoured relative to crystallization.

Acknowledgments

This work was supported by the US Department of Energy (DOE) (grant no DEFG03-97ER45654). Experiments at CRI were supported by NASA Physical Sciences Division under contract number NAS8-00125.

References

[1] Makishima A, Tamura Y and Sakaino T 1978 *J. Am. Ceram. Soc.* **61** 247
[2] Erbe E M and Day D E 1990 *J. Am. Ceram. Soc.* **73** 2708
[3] Thomas I M, Payne S A and Wilke G D 1992 *J. Non-Cryst. Solids* **151** 183
[4] Peters P M and Houde-Walter S N 1998 *J. Non-Cryst. Solids* **239** 162
[5] Maekawa H, Maekawa T, Kawamura K and Yokokawa T 1991 *J. Non-Cryst. Solids* **127** 53
[6] Ponader C W and Brown G E Jr 1989 *Geochim. Cosmochim. Acta* **53** 2893
[7] Gaskell P H, Eckersley M C, Barnes A C and Chieux P 1991 *Nature* **350** 675
[8] MaGahay V and Tomozawa M 1993 *J. Non-Cryst. Solids* **159** 246
[9] Meaker T F, Peeler D K, Marra J C, Pareizs J M and Ramsey W G 1997 Scientific basis for nuclear waste management XX *Materials Research Society Proc. (Pittsburgh, PA, 1997)* vol 465, ed W J Gray and I R Triay p 1281
[10] Feng X, Li H, Davis L L, Li L, Darab J G, Schweiger M J, Vienna J D, Bunker B C, Allen P G, Buncher J J, Craig I M, Edelstein N M, Shuh D K, Ewing R C, Wang L M and Vance E R 1999 *Ceram. Trans.* **93** 409
[11] Doremus R H 1994 *Glass Science* 2nd edn (New York: Wiley)
[12] Wilding M C and Navrotsky A 2000 *J. Non-Cryst. Solids* **265** 238
[13] Zhang Y, Navrotsky A, Li H, Li L, Davis L L and Strachan D M 2001 *J. Non-Cryst. Solids* **296** 93
[14] Delevaque E, Georges T, Monerie M, Lamouler P and Bayon J-F 1993 *IEEE Photonics Technol. Lett.* **5** 73

[15] Kohli J T and Shelby J E 1991 *Phys. Chem. Glasses* **32** 67
[16] Cho S Y, Kim I T and Hong K S 1999 *J. Mater. Res.* **14** 114
[17] Zuccaro C, Winter M, Klein N and Urban K 1997 *J. Appl. Phys.* **82** 5695
[18] Kim D-H and Kim C H 1990 *J. Am. Ceram. Soc.* **73** 1431
[19] Ekström T and Nygren M 1992 *J. Am. Cream. Soc.* **75** 259
[20] Cheng Z 1996 *J. Am. Ceram. Soc.* **79** 530
[21] Weber J K R, Felten J J and Nordine P C 1996 *Rev. Sci. Instrum.* **67** 522
[22] Navrotsky A 1977 *Phys. Chem. Minerals* **2** 89
[23] Navrotsky A 1997 *Phys. Chem. Minerals* **24** 222
[24] Ditmars D A and Douglas T B 1971 *J. Res.* A **75** 401
[25] Mraw S C 1988 *Specific Heat of Solids, CINDAS Data Series on Material Properties* vol 1, 2, ed C Y Ho (New York: Hemisphere Publishing Corporation) p 395
[26] Marezio M, Dernier P D and Remeika J P 1972 *J. Solid State Chem.* **4** 11
[27] Mizuno M, Yamada T and Noguchi T 1977 *Yogyo-Kyokai-Shi* **85** 90
[28] Mizuno M 1979 *Yogyo-Kyokai-Shi* **87** 405
[29] Coutures J P, Rifflet J C, Billard D and Coutures P 1987 Contactless treatments of liquids in a large temperature range by an aerodynamic levitation device and laser heating *Proc. 6th Eur, Symp. on Mats. in microgravity (Bordeaux Dec. 1986)*; *Eur. Space Agency, Spec. Publ. ESA* **256** 427–430
[30] Wilding M C, McMillan P F and Navrotsky A 2002 *Phys. Chem. Glasses* **43** 306
[31] Tangeman J A, Phillips B L, Nordine P C and Weber J K R 2003 Thermodynamics and structure of single- and two-phase alumina–yttria glasses *J. Phys. Chem.* B submitted
[32] Robie R A, Hemingway B S and Fisher J R 1979 Thermodynamic properties of minerals and related substances at 298.15 K and 1 bar (10^5 Pascals) pressure and at higher temperatures *US Geol. Surv. Bull. 1452*
[33] Lin I, Navrotsky A, Weber J K R and Nordine P C 1999 *J. Non-Cryst. Solids* **243** 273
[34] Kanke Y and Navrotsky A 1998 *J. Solid State Chem.* **141** 424
[35] Helean K B and Navrotsky A 2002 *J. Therm. Anal. Calorimetry* **69** 751
[36] Ray N H 1974 *J. Non-Cryst. Solids* **15** 423
[37] Geisinger K L, Oestrike R, Navrotsky A, Turner G L and Kirkpatrick R J 1988 *Geochim. Cosmochim. Acta* **52** 2405
[38] Roy B N and Navrotsky A 1984 *J. Am. Ceram. Soc.* **67** 606
[39] Navrotsky A, Geisinger K L, McMillan P and Gibbs G V 1985 *Phys. Chem. Minerals* **11** 284
[40] Ellison A J G and Hess P C 1990 *J. Geophys. Res.* **95** 717
[41] Schaller T, Stebbins J F and Wilding M C 1999 *J. Non-Cryst. Solids* **243** 146
[42] McGahay V and Tomozawa M 1993 *J. Non-Cryst. Solids* **159** 246
[43] Wang J, Brocklesby W S, Lincoln J R, Townsend J E and Payne D N 1993 *J. Non-Cryst. Solids* **163** 261
[44] Hess P C 1991 *Physical Chemistry of Magmas, Advances in Physical Geochemistry* vol 9, ed L L Perchuk and I Kushiro (New York: Springer) p 152
[45] Sen S 2000 *J. Non-Cryst. Solids* **261** 226
[46] Corrales L R 1998 *J. Non-Cryst. Solids* **242** 1
[47] Park B, Li H and Corrales L R 2000 *J. Non-Cryst. Solids* **297** 220
[48] Hillert M and Jonsson S 1992 *Z. Metallk.* **83** 720
[49] Seifert H J and Aldinger F 1996 *Z. Metallk.* **87** 841